CrystEngComm

PAPER

View Article Online
View Journal | View Issue

Cite this: *CrystEngComm*, 2023, **25**, 391

New charge-transfer complexes of 1,2,5-chalcogenadiazoles with tetrathiafulvalenes†

Elena A. Chulanova, *[ab] Ekaterina A. Radiush, [a] Yaser Balmohammadi,[c] Jens Beckmann, [d] Simon Grabowsky [c] and Andrey V. Zibarev[a]

Received 7th October 2022,
Accepted 29th November 2022

DOI: 10.1039/d2ce01385a

rsc.li/crystengcomm

Five new charge-transfer (CT) complexes of structurally varied 1,2,5-chalcogenadiazoles (monocyclic, 6-5 bicyclic and 6-6-5 tricyclic; chalcogen = S, Se and Te) with tetrathiafulvalenes (TTF and its bis(ethylenedithio) derivative BEDT-TTF) were obtained by co-crystallization of donor and acceptor components and characterized by X-ray diffraction and UV-vis spectroscopy in combination with density functional theory calculations. Bonding analyses were carried out with the quantum theory of atoms in molecules and Hirshfeld surface and non-covalent interaction analyses, accompanied by calculations of model energies of molecular pairs. According to these calculations, the complexes are rather weakly bonded by predominantly electrostatic interactions with significant contributions from dispersion interactions. The main structural motifs are assigned to π-stacking interactions and σ-hole driven hydrogen and chalcogen bonding. CT magnitudes vary between 0.09 and 0.37 e, and the CT bands in the UV-vis spectra of the complexes lie in the range of 550–750 nm.

Introduction

The charge transfer (CT) formalism[1] involving electron relocation from one molecule (donor, D) to another (acceptor, A) is a useful descriptor widely applicable in chemistry, crystal engineering and materials science, despite reasonable criticism by physics.[2] Charge transfer can be complete or incomplete. Complete CT leads to the formation of radical-ion pair salts, and incomplete CT leads to the formation of polarized molecular complexes. Within the molecular orbital (MO) theory framework, incomplete CT occurs *via* strong coupling of the D's highest occupied MO (HOMO) with the A's lowest unoccupied MO (LUMO) leading to their hybridization.[3] Despite a long history of studying intermolecular interactions, including those in crystalline CT complexes, a higher-accuracy numerical treatment, particularly based on energy decomposition analysis, has only recently been exploited as an option.[4,5]

Tetrathiafulvalenes (TTFs) and 1,2,5-chalcogenadiazoles (chalcogen = S, Se, Te) belong to the most frequently exploited D[3,6–10] and A[11–17] families, respectively. The electron-accepting ability of 1,2,5-chalcogenadiazoles is caused by positive electron affinity meaning that their radical anions (RAs) are thermodynamically more preferable than neutral molecules. With stronger electron donors/reducing agents, 1,2,5-chalcogenadiazoles afford thermally stable RA salts, and with weaker donors/reducing agents, CT complexes. Besides, these compounds reveal a unique combination of Lewis ambiphilicity, chromophoric/fluorophoric properties, and chalcogen bonding.[18–22]

In contrast to RA salts (ref. 17, 23 and 24 and references therein), CT complexes of 1,2,5-chalcogenadiazoles, including those with TTFs, are poorly studied;[25–31] beyond the complexes, hybrid TTF/1,2,5-chalcogenadiazole molecules are of fundamental and applied interest in chemistry, crystal engineering[32–37] and materials science as potential ambipolar semiconductors.[38]

Herein, we report on the synthesis and properties of new crystalline CT complexes **1–5** and **5′** between tetrathiafulvalene (TTF) (complexes **1–4**) and its bis(ethylenedithio) derivative (BEDT-TTF; complexes **5** and **5′**) and structurally varied 1,2,5-chalcogenadiazoles **6–10** (chalcogen = S, Se and Te; Scheme 1); related complexes between TTF and telluradiazole **8** and bis(thiadiazole) **11** (Scheme 1) were reported earlier.[30] Complexes **1–4** and **5′** are structurally defined by single-crystal

---

[a] *Institute of Organic Chemistry, Siberian Branch, Russian Academy of Sciences, 630090 Novosibirsk, Russia*
[b] *Institute for Applied Physics, University of Tübingen, 72076 Tübingen, Germany. E-mail: elena.chulanova@uni-tuebingen.de*
[c] *Department of Chemistry, Biochemistry and Pharmaceutical Sciences, University of Bern, 3012 Bern, Switzerland*
[d] *Institute for Inorganic Chemistry and Crystallography, University of Bremen, 28359 Bremen, Germany*

† Electronic supplementary information (ESI) available: Data of single-crystal and powder XRD and HS analysis. CCDC 2192018 (**1**), 2192019 (**2**), 2192020 (**3**), 2192021 (**4**) and 2192022 (**5′**). For ESI and crystallographic data in CIF or other electronic format see DOI: **https://doi.org/10.1039/d2ce01385a**

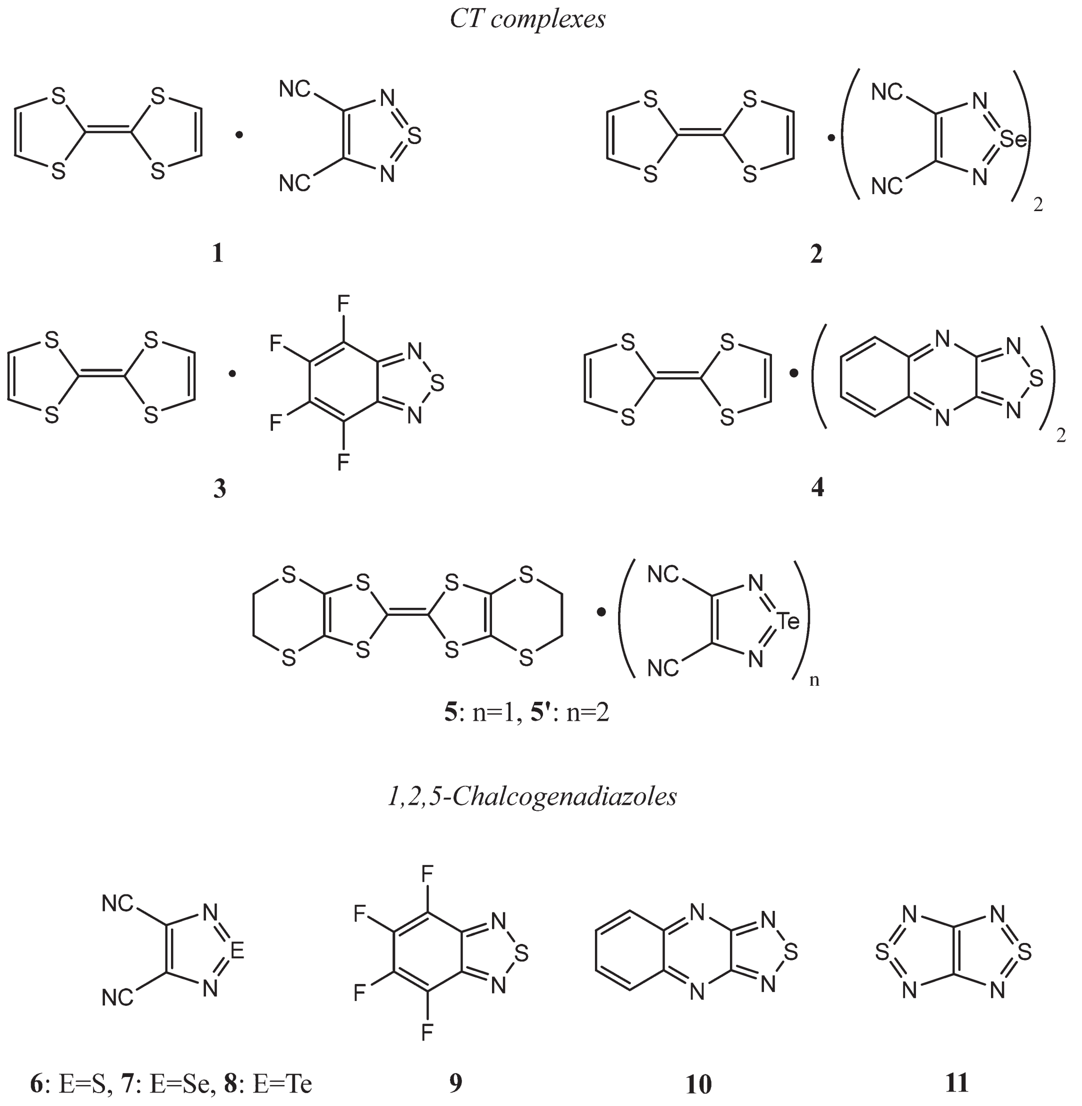

Scheme 1 CT complexes **1–5** and **5′** between TTF and BEDT-TTF, and 1,2,5-chalcogenadiazoles **6–11**.

X-ray diffraction (XRD), together with Hirshfeld surface (HS) analysis,[39] accompanied by density functional theory (DFT) calculations of the model energies of molecular pairs.[40,41] Their electronic structures and bonding situations are studied by DFT calculations and quantum theory of atoms in molecules (QTAIM) analysis[42] as well as non-covalent interaction (NCI) index calculations,[43,44] and for **1–4** also by UV-vis spectroscopy (for **5′**, measurements were impossible due to low solubility). Despite numerous attractive secondary bonding interactions (SBIs) observed in their crystal structures, the complexes are rather weakly bonded; theoretically estimated CT magnitudes are relatively low.

Experimental and computational section

General

TTF and BEDT-TTF were obtained from Aldrich and used as received. Compounds **6–10** were prepared by known methods.[45–49] Solvents were dried by common drying agents and redistilled. Elemental analyses for C, H and N were performed with a CHNS-analyzer Euro EA 3000. UV-vis spectra were measured with an SF 2000 instrument.

Synthesis

Complexes 1–4. A 1 : 1 mixture of compound **6**, **7**, **9** or **10** with TTF was dissolved in a minimal volume of chloroform. The resulting dark colored solutions were evaporated under a stream of argon. Complexes **1–3** were obtained quantitatively in the form of black powders. Complex **1**: found, %: C, 34.96; H, 1.12; N, 17.15; calculated for $C_{10}H_4N_4S_5$, %: C, 35.28; H, 1.18; N, 16.46. Complex **2**: found, %: C, 29.42; H, 0.72; N, 19.57; calculated for $C_{14}H_4N_8S_4Se_2$, %: C, 29.48; H, 0.71; N, 19.64. Complex **3**: found, %: C, 35.00; H, 1.02; N, 6.75; calculated for $C_{12}H_4F_4N_2S_5$, %: C, 34.94; H, 0.98; N, 6.79. Complex **4** could not be obtained in pure form according to elemental analysis due to partial decomposition of **10** in solution during the crystallization process both under ambient and anaerobic conditions. Single crystals of **1–4** suitable for XRD were obtained from dichloromethane solutions at −4 °C.

Complexes 5 and 5′. Under argon, a 1 : 1 mixture of compound **8** and BEDT-TTF (0.12 mmol) was refluxed in 2 ml of chloroform for 15 min. The resulting black precipitate was filtered off and washed with chloroform. Complex **5** (92%); found, %: C, 27.06; H, 1.30; N, 9.48; calculated for $C_{14}H_8N_4S_8Te$, %: C, 27.28; H, 1.31; N, 9.09. Slow evaporation of either 1 : 1 or 1 : 2 suspensions of BEDT-TTF and **8** in acetonitrile gave a mixture of complex **5′** with the starting materials; crystals of **5′** suitable for XRD were separated mechanically.

X-ray diffraction

Single-crystal XRD measurements of complexes **1–4** and **5′** (see the ESI†) were carried out with a Bruker Venture D8 diffractometer using graphite-monochromated Mo Kα radiation (λ = 0.71073 Å). The structures were solved by direct methods using SHELX-97 and Olex2 1.2 programs[50,51] and refined by the full-matrix least-squares method against all F^2 with anisotropic displacement parameters for non-hydrogen atoms using the SHELXL-2018/3 program.[52] The hydrogen atoms' positions were calculated with the riding model. Absorption corrections were applied using the empirical multiscan method with the SADABS program.[53] The crystal structures obtained were analyzed for shortened contacts between non-bonded atoms using the MERCURY program.[54] CCDC 2192018 (**1**), 2192019 (**2**), 2192020 (**3**), 2192021 (**4**) and 2192022 (**5′**) contain the supplementary crystallographic data for this paper.

Powder XRD data were collected with a Bruker D8 Advance instrument equipped with a Lynx-Eye detector (Cu K_α radiation, λ = 1.54184 Å). Data were collected within the 2θ range of 5–40° with a scanning step of 0.03° and an accumulation time of 1 s. Modeling of the diffraction patterns from the single-crystal structures was performed using the MERCURY program.[54]

Quantum chemical calculations

The geometries of complexes **1–4** and **5′** were optimized at the B97-D3 level of theory[55,56] with the def2-tzvp basis set[57,58] with an effective core potential (ECP) for Te. The Becke–Johnson damping function was used in all dispersion-corrected calculations.[59] The Grimme geometrical counterpoise (gCP) correction scheme was applied for a semiempirical account of the basis-set superposition error (BSSE) effects.[60] The energy of the bonding interaction E_b was calculated as the difference between the energy of the complex (E_{cplx}) and the sum of the energies of the corresponding 1,2,5-chalcogenadiazole (E_{het}) and TTF/BEDT-TTF (E_{ttf}) units corrected for the BSSEs and zero-point vibrational energies (ZPEs) using the following equation: $E_b = -(E_{cplx} - E_{het} - E_{ttf} + E_{BSSE} + \Delta E_{ZPE})$. The CT value was calculated as the loss of the net charge on the TTF/BEDT-TTF moieties.

The UV-vis spectra of the complexes were calculated using their optimized geometries at the TD-DFT level of theory[61] with the double-hybrid B2PLYP method,[62] the def2-tzvp basis set and an ECP for Te by applying the COSMO solvation model.[63,64] The RIJCOSX approximation was used to speed up computations with hybrid functionals.[65,66] All aforementioned DFT calculations were performed with the ORCA suite of programs (version 4.0.1.2).[67]

The B3LYP functional[68–70] and def2-tzvp basis set with an ECP for Te were used for vertical ionization energy calculations performed with the Gaussian 09 (ref. 71) suite of programs.

The B97-D3/def2-tzvp densities were used in QTAIM and NCI index analyses, performed with the Multiwfn program (version 3.2).[72] The NCI isosurfaces of the complexes were plotted using the VMD software for $s(r)$ = 0.5, color range of $\lambda_2 \cdot \rho$ from −0.03 to 0.03.[73]

HS analyses were performed with the CrystalExplorer program.[74] The DFT calculations of the model energies of molecular pairs were carried out with Gaussian09 (ref. 71) as interfaced with CrystalExplorer at the B3LYP level of theory[75] with 6-31(d,p)[75] and dgdzvp[76,77] basis sets.

Results and discussion

Synthesis

For the synthesis of new CT complexes, TTF and BEDT-TTF were used as D's, and 1,2,5-chalcogenadiazoles **6–10** as A's (Scheme 1). The complexes **1–4** were prepared by co-crystallization of the components from chloroform. In the case of BEDT-TTF and **8**, fast precipitation afforded 1 : 1 complex **5** even when the initial molar ratio of the components in solution was 1 : 2, whereas slow evaporation gave the expected 1 : 2 complex **5′** (*cf.* ref. 30).

According to the DFT calculations at the B3LYP level of theory, the first adiabatic ionization energy of TTF and BEDT-TTF is 6.20 and 5.91 eV, respectively, whereas the first adiabatic electron affinity of chalcogenadiazoles varies from 1.57 for **9** to 2.21 eV for **10**.[17] For the CT complexes of S and Se containing A's **6**, **7**, **9** and **10**, a normal 1 : 1 stoichiometry should be expected, whereas for the complex of Te containing **8**, a 1 : 2 stoichiometry is expected due to the special propensity of telluradiazoles to σ-hole driven SBIs in the form of chalcogen bonding *via* shortened Te⋯N intermolecular contacts (see ref. 18–21 and 30 and references therein).

XRD, HS and NCI analyses

Complexes **1–4** and **5′** were structurally characterized by single-crystal XRD (Fig. 1, Table S1, ESI†); complex **5** was unsuitable for XRD, and its stoichiometry was determined by elemental analysis. The structural authenticity of low-crystalline bulky samples was controlled with powder XRD (ESI†). Crystalline complexes **1–4** and **5′** reveal layered structures with alternating D and A molecules forming π-stacks; the peculiarity of **4** is that the π-stacks are formed by an A–D–A motif (Fig. 1). In **1**, the layers contain alternating infinite ribbons of TTF and head-to-tail arranged molecules of **6** with S$\cdots$N contacts equal to 3.135(5) and 3.267(5) Å (the sum of van der Waals (vdW) radii is 3.55 Å).[78] Hydrogen bonds are observed between H atoms of TTF and N atoms of CN groups (2.738 and 2.533 Å) or the heterocycle (2.574 and 2.705) of **6**; the interlayer distances are equal to 3.27–3.39 Å (the interlayer distances in graphite are equal to 3.35 Å).[79]

In complex **2**, neighboring stacks of infinite ribbons of TTF and **7** are tilted by 44.9°. Ribbons of **7** consist of pairs of heterocycles forming [Se$\cdots$N]$_2$ tetragons with intermolecular Se$\cdots$N contacts of 2.833(1) and 2.891(1) Å (the sum of vdW radii is 3.52 Å).[78] Hydrogen bonds are observed between H atoms of TTF and N atoms of CN groups (2.471 and 2.570 Å) of **7**; the interlayer distances are 3.21–3.42 Å. In complex **3**, neighboring π-stacks are tilted by 53.3°; D and A molecules alternate in the stacks and layers, and the interlayer distances are 3.42–3.55 Å. Shortened contacts are observed between an S atom of **9** and two F atoms from the neighboring stack, the contact distances are 3.079(2) Å (the sum of vdW radii is 3.35 Å).[78] Hydrogen bonds are observed between H atoms of TTF and N atoms of the heterocycle (2.565 and 2.713) of **9**.

In complex **4**, π-stacks are tilted by 30.2° with a small offset of neighboring molecules; the interplanar separations in the stacks are 3.37–3.40 Å. Shortened contacts are observed between an S atom of **10** and an N atom of the pyrazine ring of **10** from the neighboring stack. The contact distance is 3.222(2)

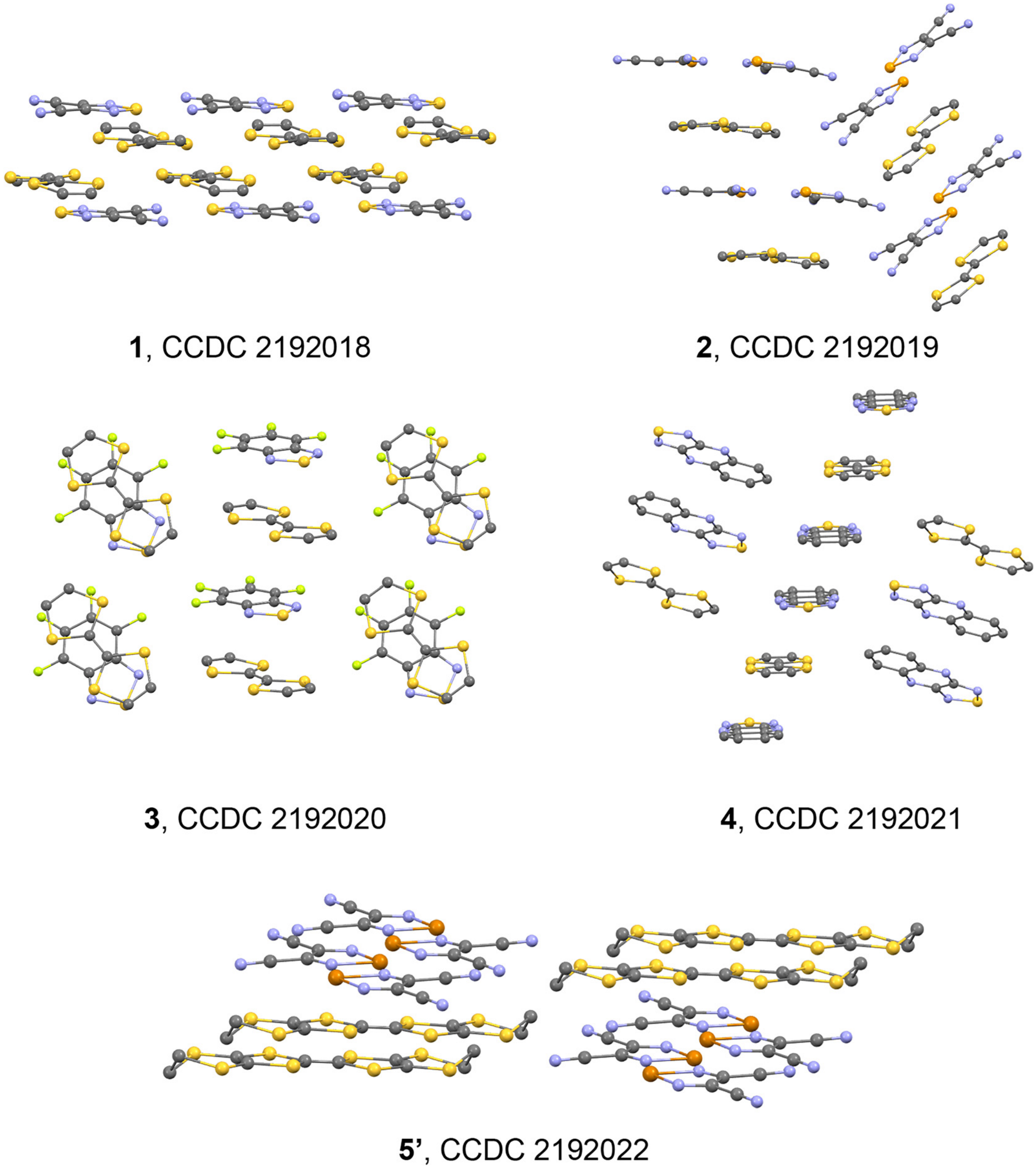

1, CCDC 2192018

2, CCDC 2192019

3, CCDC 2192020

4, CCDC 2192021

5', CCDC 2192022

Fig. 1 XRD crystal structures of CT complexes **1**–**4** and **5'**, H atoms are omitted for clarity. Color code: C – grey, F – green, N – blue, S – yellow, Se – orange, Te – dark orange.

Å (the sum of vdW radii is 3.55 Å).[78] Hydrogen bonds are observed between H atoms of TTF and N atoms of the pyrazine ring of **10**. The contact distance is 2.609 Å, and between the H and N atoms of the heterocycle of **10**, the contact distance is 2.575 Å. The packing of complex **5′** featuring infinite ribbons of BEDT-TTF and **8** is similar to that of a previously studied complex between TTF and **8** (ref. 30): molecules of **8** form chains with Te···N contacts of 2.727(2) and 2.680(2) Å (the sum of vdW radii is 3.65 Å)[78] where they are slightly shifted out of the mean layer plane (CN groups, by 0.1 Å). Hydrogen bonds are observed between H atoms of BEDT-TTF and N atoms of the CN groups (2.526 and 2.615 Å) of **8**. The interlayer distances in **5′** are equal to 2.93–3.22 Å, being slightly shorter than those in the complex of **8** with TTF.[30]

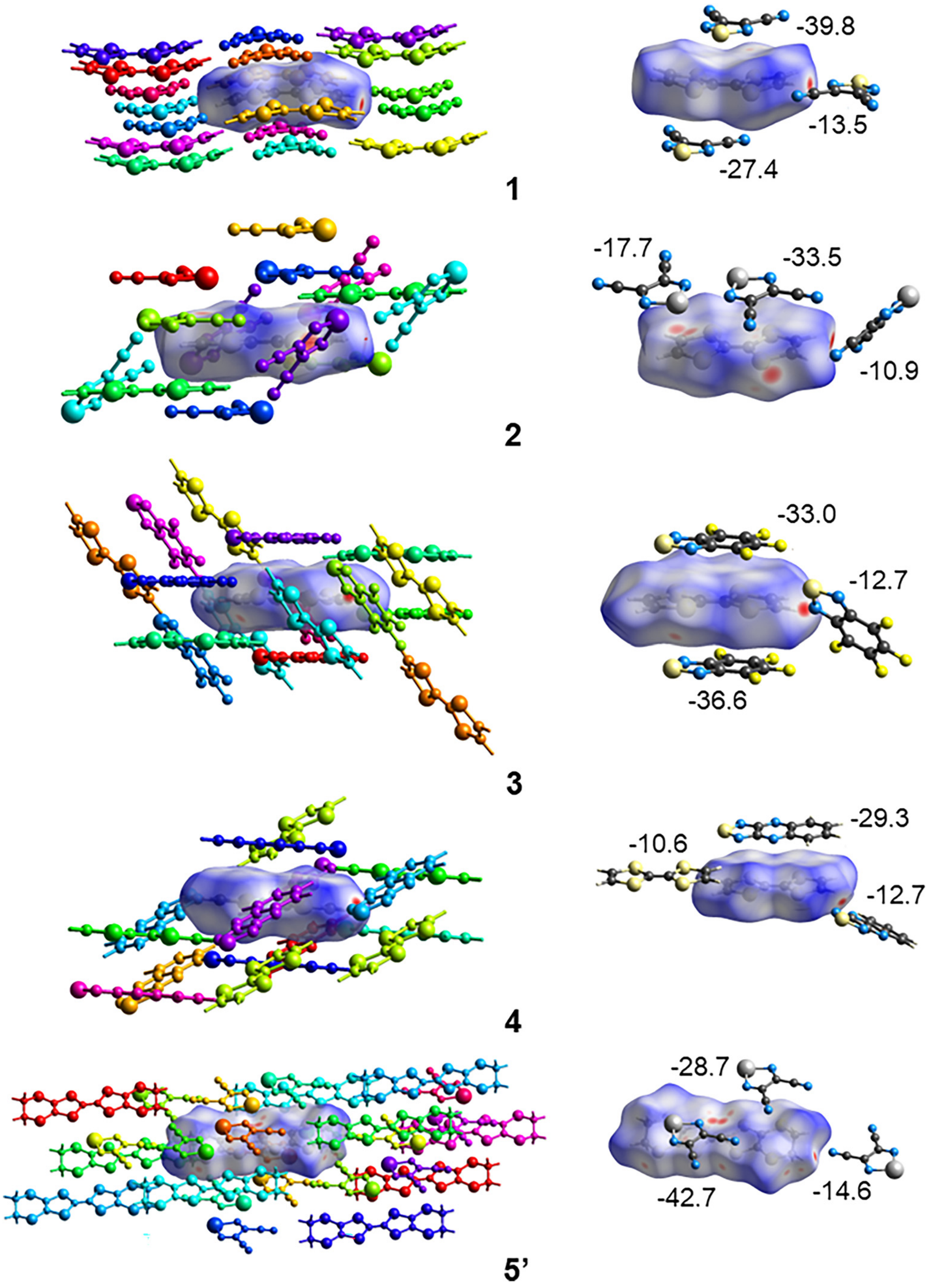

Fig. 2 HSs of complexes **1**–**4** and **5′** mapped with d_{norm},[88] together with the closest neighbors (left column, for color code see Table 1) and together with those neighbors that have the highest interaction energies (shown in kJ mol^{-1}) with the reference molecule. The HS colour code: red – the distance *R* between the closest atoms inside and outside a surface point is smaller than the sum of their vdW radii; blue – *R* is larger than the sum of the vdW radii; white – *R* is approximately equal to the sum of the radii.

Table 1 Interaction energy and its components (kJ mol^{-1}) for complexes **1**–**4** and **5′** calculated at the B3LYP level of theory with 6-31(d,p)/dgdzvp basis sets.[a,b,c] The reference molecule below the HS and the color-coded neighboring molecules are depicted in Fig. 2, left column

	E_{ele}	E_{pol}	E_{dis}	E_{rep}	E_{tot}
			1		
🟦	–29.1 / –40.8	–4.4 / –4.7	–43.6[b]	57.7 / 72.6	–36.4 / –39.8
🟦	–16.2 / –25.8	–3.8 / –4.0	–35.7[b]	42.7 / 55.0	–24.6 / –27.4
🟩	–7.0 / –10.6	–0.8 / –0.8	–12.2[b]	9.1 / 14.5	–13.0 / –13.5
🟩	–4.9 / –8.2	–0.7 / –0.8	–9.7[b]	6.2 / 11.3	–10.3 / –10.7
			2		
🟦	–21.2 / –31.6	–3.6 / –3.8	–38.0[b]	41.3 / 58.1	–32.7 / –33.5
🟥	–14.4 / –23.0	–2.2 / –2.4	–23.3[b]	31.9 / 46.3	–17.5 / –17.7
🟦	–9.7 / –11.5	–1.6 / –1.6	–9.3[b]	14.3 / 17.0	–10.7 / –10.9
🟩	–8.5 / –9.9	–0.9 / –0.8	–9.8[b]	12.8 / 15.1	–10.2 / –10.2
			3		
🟥	–16.9 / –33.0	–2.5 / –2.8	–49.0[b]	51.7 / 69.5	–30.5 / –36.6
🟪	–14.6 / –25.2	–2.1 / –2.3	–41.7[b]	38.8 / 51.2	–29.3 / –33.0
🟩	–10.9 / –13.7	–1.4 / –1.6	–11.4[b]	16.3 / 19.8	–12.5 / –13.3
🟩	–10.1 / –12.5	–1.5 / –1.6	–9.9[b]	13.7 / 16.7	–12.0 / –12.7
🟨	–5.7 / –7.2	–0.9 / –0.9	–9.5[b]	8.1 / 10.5	–10.0 / –10.0
			4		
🟪	–12.5 / –27.8	–2.3 / –2.3	–50.4[b]	53.1 / 73.9	–26.0 / –29.3
🟦	–7.9 / –10.0	–2.6 / –2.8	–10.2[b]	11.7 / 14.3	–11.9 / –12.7
🟩	–5.9 / –7.5	–0.9 / –0.9	–8.9[b]	7.2 / 9.2	–10.1 / –10.6
			5’[c]		
🟧	–47.3	–4.4	–43.5	78.4	–42.7
🟩	–22.1	–3.1	–29.6	36.9	–28.7
🟧	–21.2	–3.2	–28.3	48.8	–19.2
🟩	–13.7	–1.5	–14.0	18.5	–16.4
🟩	–14.4	–2.6	–6.5	13.1	–14.7
🟩	–8.2	–1.4	–10.3	7.2	–14.2

[a] E_{tot} is the total interaction energy (only values ≥|10| kJ mol^{-1} are shown; for the full version of this table, see the ESI†); E_{ele}, E_{pol}, E_{dis} and E_{rep} are energies of the electrostatic, polarization, dispersion and Pauli-repulsion interactions, respectively. E_{ele}, E_{pol}, E_{dis} and E_{rep} are given as absolute values without scale factor, whereas E_{tot} is the sum of the scaled[41] components. [b] The dispersion energies are independent of the level of theory as they are taken as sums of tabulated atomic Grimme terms. [c] For **5′**, only B3LYP/dgdzvp data are given because for the element Te, the basis set 6-31G(d,p) is not defined.

In crystalline complex **1**, the geometry of acceptor **6** does not differ from that in its homocrystals.[80] For complexes **2** and **4**, however, the C–N bond lengths in the chalcogenadiazole rings of acceptors **7** and **9** are shortened by 0.013 Å and 0.033 Å, respectively, as compared with the XRD structures of the individual heterocycles.[80,81] In complex **5′**, the Te–N bond length of **8** is shortened by 0.010 Å, while all other parameters remain almost the same as in the individual telluradiazole.[82]

While in TTF homocrystals, terminal C atoms are coplanar with the neighboring S atoms and deviate from the plane containing all four S atoms of the molecule by only 2.1°,[83] in complex **1**, TTF molecules have an asymmetrical boat-shape conformation with the aforementioned angle equal to 10.67° and 12.59°. In complex **2**, one of the crystallographically non-identical TTF molecules has the same conformation with C atoms deviating by 9.52° and 4.45° at its opposite sides. A similar pattern is observed for complex **3** featuring deformation angles of 3.09° and 6.11°. In complex **4**, the geometry of the TTF molecules is close to planarity with a deformation angle of 1.08°. In complex **5′**, BEDT-TTF molecules are flattened as compared with BEDT-TTF homocrystals.[84]

Hirshfeld surface (HS) analysis[39,85–88] of the XRD structures of complexes **1–4** and **5′**, conducted with TTF as the reference for **1–4** and BEDT-TTF for **5′**, revealed that the closest contact between the two components in all complexes is the classical N⋯H hydrogen bond.[89,90] This bond is quite strong but it is not the strongest SBI observed in the crystal packing of **1–4** and **5′**. According to the DFT calculations of the model energies of molecular pairs (taken as the sum of scaled electrostatic, polarization, dispersion and Pauli-repulsion interaction terms: $E_{\mathrm{tot}} = E_{\mathrm{ele}} + E_{\mathrm{pol}} + E_{\mathrm{dis}} + E_{\mathrm{rep}}$)[40] (Fig. 2, Table 1), for complexes **1–3** and **5′**, the strongest SBIs are π-stacking interactions. This can also be observed in NCI iso-surfaces as long-ranging light-green regions between the molecules (Fig. 3); S⋯S (**1**, **3**), Se⋯S (**2**) or Te⋯S (**5′**) chalcogen bonding interactions (*i.e.*, incarnations of σ-hole driven SBIs)[18–21,91–97] are also significant. For complex **4**, the strongest SBI is also π-stacking but there are no S⋯S intermolecular contacts in distances less than the sum of the vdW radii.

For both π-stacking and chalcogen bonding interactions, the dispersion energy term dominates over the electrostatic term (Table 1). This dominance of dispersion interactions is also obvious in the NCI representations (Fig. 3). In general, chalcogen bonding is an attractive interaction featuring contributions of electrostatic, CT and dispersion terms to variable extents; the CT contribution is associated with an

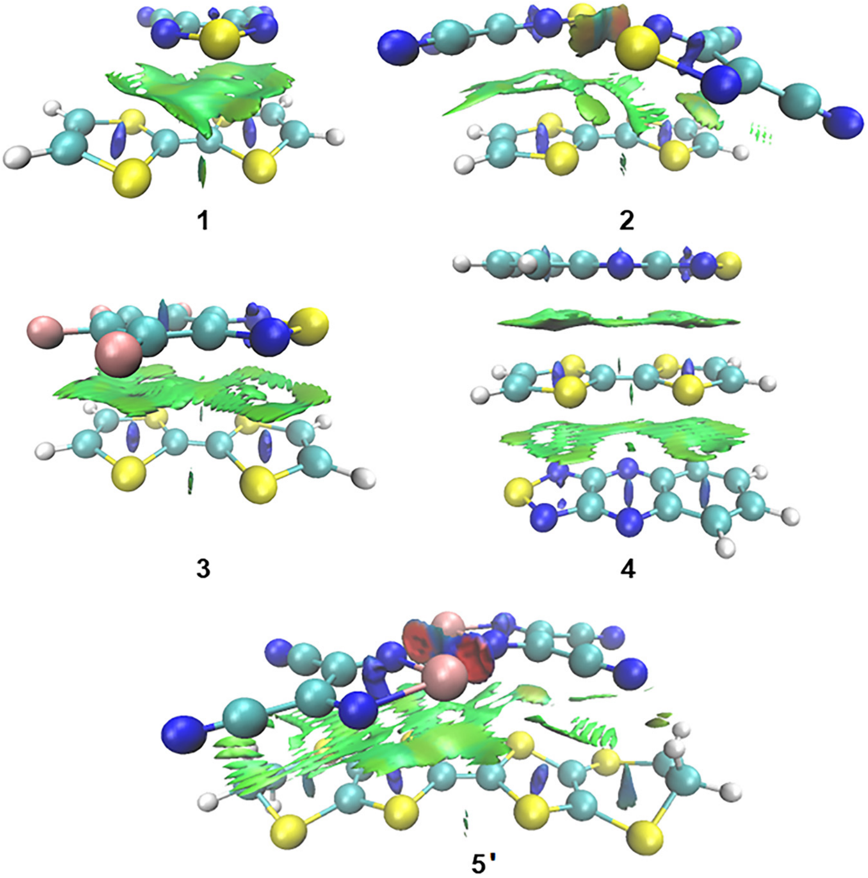

Fig. 3 NCI iso-surfaces at $s(r) = 0.5$ for complexes **1–4** and **5′** (color code for $\lambda_2 \cdot \rho$ ranges from −0.03 to 0.03; blue = attractive, red = repulsive, green-brown = weakly attractive vdW type).

interaction of the occupied MO of the D molecule (the chalcogen bond acceptor) with the virtual σ*-MO of an A molecule (the chalcogen bond donor);[96] *cf.* Alcock model.[98]

CT and QTAIM analyses

For 0.1 M chloroform solutions of complexes **1–4**, a new broad long-wavelength absorption band (around 550 nm for **1** and **3**, 600 nm for **2**, and 750 nm for **4**) was observed in the UV-vis spectra in comparison with those of the individual components (Fig. 4; for complex **5′** measurements were impossible due to low solubility). On diluting to 0.05 M, this band disappears in the spectrum of complex **3**, and on further diluting, in the spectra of complexes **1**, **2** and **4**, indicating that they are weakly bonded in solution. According to TD-DFT calculations (Table 2), the discussed band mostly corresponds to the electron promotion from the HOMO localized mostly on the TTF molecule onto the LUMO localized mostly on 1,2,5-chalcogenadiazole (Fig. 5), *i.e.*, it is the CT band. Numerical agreement between theory and experiment is, however, satisfactory only for **1** and **3**, whereas for **2** and **4** the calculated λ_{CT} values are too large (Table 2).

In vacuo structures of complexes **1–4** and **5′** optimized at the B97-D3 level of DFT (Fig. 5) are close to their structures in the respective crystals. According to the calculations, CT from TTF/BEDT-TTF onto chalcogenadiazoles varies from 0.09 e in **3** to 0.37 and 0.33 e in **4** and **5′**, respectively. These CT values correlate with previously reported calculated electron affinities of the corresponding chalcogenadiazoles.[17] The energies of bonding interactions in the complexes lie in the range E_b = 58–192 kJ mol^{-1} (Table 2; *cf.* Table 1). They are lower than E_b of 102–328 kJ mol^{-1} in the anionic complexes of **7** and **8** featuring E⋯X$^-$ (E = Se, Te; X = PhS$^-$, F$^-$, I$^-$) chalcogen bonding.[21,80,99,100] The QTAIM[101,102] analysis reveals bond critical points[103] (BCPs) between D and A moieties in all complexes (Fig. 5) characterized by low values of electron density ρ_b and its Laplacian $\nabla^2\rho_b$ (Table 2). Values of $\rho_b < 0.1$ and small and positive values of $\nabla^2\rho_b$ characterize interactions of molecules with closed-shell electronic configurations, *i.e.*, mostly electrostatic interactions.[104,105] Additionally, for all BCPs, $|V_b|/G_b < 1$ (Table 2), which is typical of SBIs[106] and corresponds to predominantly electrostatic interaction. These values are in the same range as for complexes of **8** with various anions.[99,107–109] Overall, QTAIM, HS and NCI analyses jointly suggest that the most important contributions to E_{tot} are E_{dis} and E_{ele} with varied relative significance (Tables 1 and 2, Fig. 2, 3 and 5). π-Stacking arrangements and the dominance of dispersion interactions are typical for CT complexes.[110]

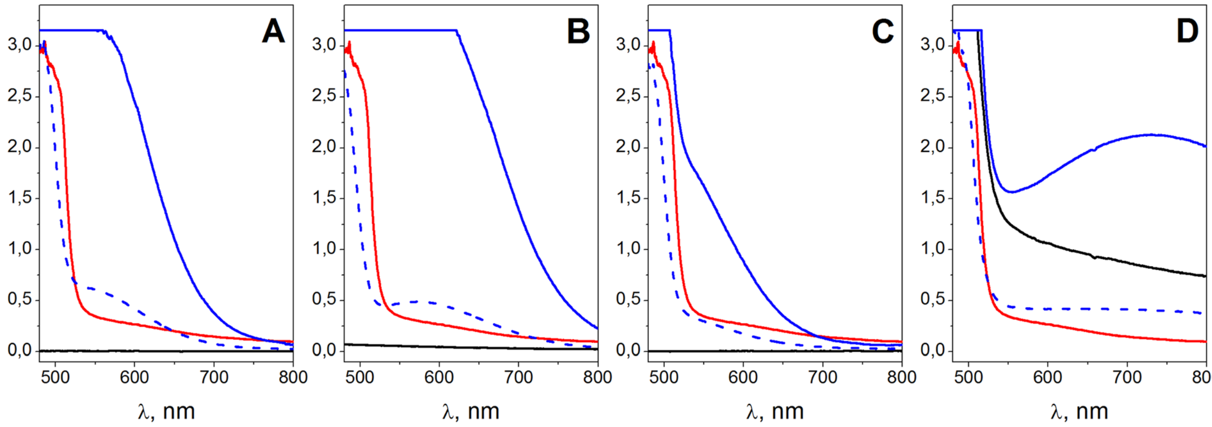

Fig. 4 UV-vis spectra of 0.1 M chloroform solutions of individual TTF (red lines) and compounds **6**, **7**, **9** and **10** (A–D, respectively; black lines), and their mixtures at 0.1 and 0.05 M concentrations (solid and dashed blue lines, respectively).

Table 2 DFT-calculated[a] energies of bonding interactions E_b, CT between D and A components, λ_{CT} of the electronic transitions in comparison with measurement, and QTAIM topological descriptors of the complexes

Complex	E_b, kJ mol^{-1}	CT,[b] e	λ_{CT},[c] nm		QTAIM descriptors[d]		
			DFT	UV-vis	ρ_b, e a_o^{-3}	$\nabla^2\rho_b$, e a_o^{-5}	$\lvert V_b\rvert/G_b$
1	65.6	0.15/0.13	616	550	0.005–0.009	0.016–0.025	0.685–0.764
2	127.1	0.29/0.29	1068	600	0.005–0.011	0.017–0.029	0.681–0.857
3	58.1	0.09/0.04	453	550	0.004–0.008	0.014–0.021	0.670–0.785
4	130.4	0.37/0.35	1391	750	0.005–0.009	0.017–0.023	0.656–0.812
5′	191.9	0.33/0.36	864	—	0.003–0.012	0.014–0.039	0.605–0.867

[a] B97-D3/def2-tzvp with ECP for Te. [b] Taken as the difference of AIM/Mulliken charges of D and A components of a complex, for complexes **1** and **3** with 1 : 1 stoichiometry, per molecule, and for **2**, **4** and **5′** with 1 : 2 stoichiometry, per one D molecule and two A molecules. [c] Measured and calculated at the TD-B2PLYP/def2-tzvp level with ECP for Te for solutions in $CHCl_3$. [d] Electron density ρ_b, its Laplacian $\nabla^2\rho_b$, and absolute values of the ratio of potential (V_b) and kinetic (G_b) energy densities at bond critical points of the complexes' bond paths.

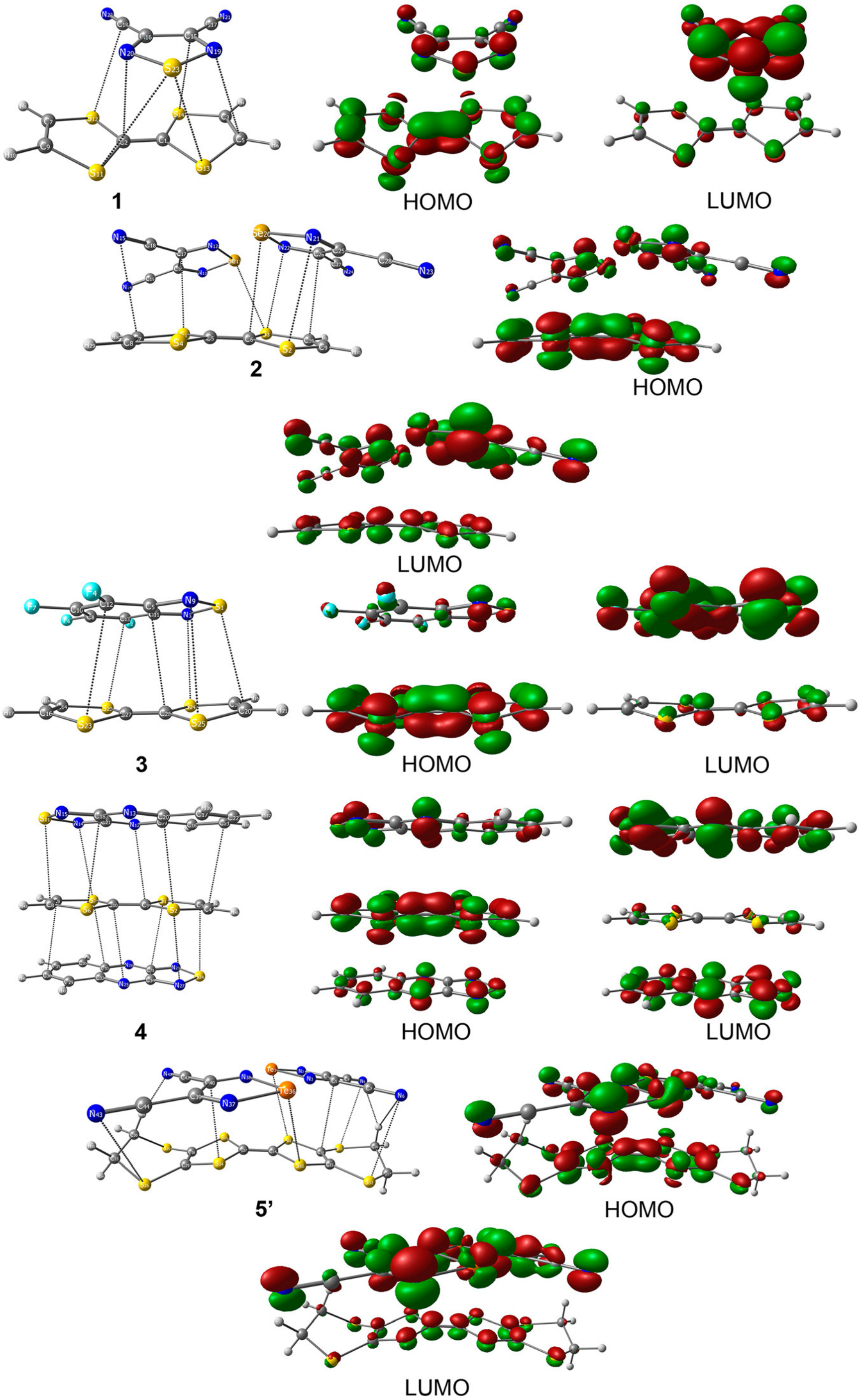

Fig. 5 *In vacuo* structures of complexes **1**–**4** and **5′** optimized at the B97-D3/def2-tzvp level, and their frontier MOs. Dashed lines indicate bond paths with BCPs between D's and A's.

Previously studied CT complexes between TTF and **8** as well as **11** displayed semiconductor properties with an activation energy of 0.40 and 0.34 eV, respectively, in the single-crystalline state and photoconductive effects with increased conductivity under white-light illumination in the polycrystalline-film state.[30] Polycrystalline films of complexes **1**–**3**, whose authenticity was confirmed by powder XRD, were unstable over time, *i.e.*, decomposed while being kept under ambient conditions within several days. Freshly prepared, they revealed weak semiconductor conductivity ($\sigma_{RT} \sim 10^{-7}$ S cm^{-1}) slightly increasing upon white-light illumination. Complex **3** displayed a small positive gate voltage effect suggesting p-type behaviour. The structural variability of both TTFs and 1,2,5-chalcogenadiazoles, together with the possibility of fine tuning their stereoelectronic properties, supports the relevance for further synthetic and crystal engineering efforts in this field.

Conclusions

Five new crystalline CT complexes between tetrathiafulvalenes (TTF and its bis(ethylenedithio) derivative BEDT-TTF) and structurally varied 1,2,5-chalcogenadiazoles (mono-, 6-5 bi- and 6-6-5 tricyclics; chalcogen = S, Se and Te) have been prepared and structurally and functionally characterized to join this recently established family of CT complexes. Despite numerous attractive secondary bonding interactions, the complexes are rather weakly bonded by predominantly electrostatic interactions (mostly hydrogen bonds) with significant contributions from dispersion interactions (mostly π-stacking and chalcogen-bonding interactions). The charge transfer varies between 0.09 and 0.37 e, and the corresponding absorption band in the UV-vis spectra lies in the range of 550–750 nm. In the form of freshly-prepared polycrystalline thin films, the complexes revealed weak, dark photosemiconductor conductivity. The large structural variability of both tetrathiafulvalene donors and 1,2,5-chalcogenadiazole acceptors suggests that further synthetic and crystal engineering efforts in this field might be fruitful. The most straightforward lead will be the stabilization of CT complexes *via* SBI strengthening. To this end, *a priori* quantum chemical modeling is the most important technique. A particular attention can be paid to heavier chalcogen-associated dispersion interactions[111,112] as the driving force, and to Se and Te congeners of TTFs[113] and 1,2,5-selena/telluradiazoles as D and A structural blocks.

Conflicts of interest

There are no conflicts to declare.

Acknowledgements

The authors are grateful to Prof. Neil Robertson and Dr. Helen Benjamin (Edinburg University, UK) for preliminary electrical measurements on the complexes, to Dr. Dmitry A. Yatsenko (Boreskov Institute of Catalysis, Russia) for powder XRD measurements, to the Deutsche Forschungsgemeinschaft (project no. BE 3716/6-2) and to the Grant program of the President of the Russian Federation (project no. MK-1533.2021.1.3) for financial support of this work. We also thank the multi-access Chemical Research Centre and Siberian Supercomputer Centre, Siberian Branch of the Russian Academy of Sciences, for instrumental and computational facilities.

Notes and references

1 R. S. Mulliken, *J. Am. Chem. Soc.*, 1952, **74**, 811–824.

2 C. B. Aakeroy, S. Alavi, L. Brammer, D. L. Bryce, T. Clark, J. E. Del Bene, A. J. Edwards, C. Esterhuysen, T. N. G. Row, P. Kennepohl, A. C. Legon, G. O. Lloyd, J. S. Murray, W. T. Pennington, P. Politzer, K. E. Riley, S. V. Rosokha, S. Scheiner, S. Tsuzuki and I. Vargas-Baca, *Faraday Discuss.*, 2017, **203**, 131–163.

3 K. P. Goetz, D. Vermeulen, M. E. Payne, C. Kloc, L. E. McNeil and O. D. Jurchescu, *J. Mater. Chem. C*, 2014, **2**, 3065–3076.

4 J. D. Wright, *Molecular Crystals*, Cambridge University Press, 1994.

5 M. J. S. Phipps, T. Fox, C. S. Taufermann and C.-K. Skylaris, *Chem. Soc. Rev.*, 2015, **44**, 3177–3211.

6 J. Yamada and T. Sugimoto, *TTF Chemistry: Fundamentals and Applications of Tetrathiafulvalene*, Springer-Verlag, 2004.

7 G. Schukat, A. M. Richter and E. Fanghänel, *Sulfur Rep.*, 1987, **7**, 155–231.

8 G. Schukat and E. Fanghänel, *Sulfur Rep.*, 1996, **18**, 1–278.

9 M. R. Bryce and L. C. Murphy, *Nature*, 1984, **309**, 119–126.

10 Y. Ihara and S. Imajo, *Crystals*, 2022, **12**, 711.

11 E. Tanaka, M. S. Mikhailov, N. S. Gudim, E. A. Knyazeva, L. V. Mikhalchenko, N. Robertson and O. A. Rakitin, *Mol. Syst. Des. Eng.*, 2021, **6**, 730–738.

12 A. Leventis, T. N. Chmovzh, E. A. Knyazeva, Y. Han, M. Heeney, O. A. Rakitin and H. Bronstein, *Polym. Chem.*, 2020, **11**, 581–585.

13 V. M. Korshunov, T. N. Chmovzh, E. A. Knyazeva, I. V. Taydakov, L. V. Mikhalchenko, E. A. Varaksina, R. S. Saifutyarov, I. C. Avetissov and O. A. Rakitin, *Chem. Commun.*, 2019, **55**, 13354–13357.

14 E. A. Knyazeva, W. Wu, T. N. Chmovzh, N. Robertson, J. D. Woollins and O. A. Rakitin, *Sol. Energy*, 2017, **144**, 134–143.

15 Y. Wang and T. Michinobu, *J. Mater. Chem. C*, 2016, **4**, 6200–6214.

16 E. A. Knyazeva and O. A. Rakitin, *Russ. Chem. Rev.*, 2016, **85**, 1146–1183.

17 A. V. Lonchakov, O. A. Rakitin, N. P. Gritsan and A. V. Zibarev, *Molecules*, 2013, **18**, 9850–9900.

18 A. F. Cozzolino, P. J. W. Elder and I. Vargas-Baca, *Coord. Chem. Rev.*, 2011, **255**, 1426–1438.

19 P. C. Ho, J. Z. Wang, F. Meloni and I. Vargas-Baca, *Coord. Chem. Rev.*, 2020, **422**, 213464.

20 E. A. Chulanova, E. A. Radiush, I. K. Shundrina, I. Yu. Bagryanskaya, N. A. Semenov, J. Beckmann, N. P. Gritsan and A. V. Zibarev, *Cryst. Growth Des.*, 2020, **20**, 5868–5879.

21 E. R. T. Tiekink, *Coord. Chem. Rev.*, 2022, **457**, 214397.

22 B. A. D. Neto, J. R. Correa and J. Spencer, *Chem. – Eur. J.*, 2022, **28**, e202103262.

23 A. V. Zibarev, in *Chalcogen Chemistry: Fundamentals and Applications*, ed. V. Lippolis, C. Santi, E. J. Lenardao and A. L. Braga, Royal Society of Chemistry, 2023, pp. 168–186.

24 N. A. Semenov, E. A. Radiush, E. A. Chulanova, A. M. Z. Slawin, J. D. Woollins, E. M. Kadilenko, I. Yu. Bagryanskaya, I. G. Irtegova, A. S. Bogomyakov, L. A. Shundrin, N. P. Gritsan and A. V. Zibarev, *New J. Chem.*, 2019, **43**, 16331–16337.

25 T. Suzuki, C. Kabuto, Y. Yamashita and T. Mukai, *Bull. Chem. Soc. Jpn.*, 1987, **60**, 2111–2115.

26 G. Berionni, A.-M. Gonçalves, C. Mathieu, T. Devic, A. Etchéberry and R. Goumont, *Phys. Chem. Chem. Phys.*, 2011, **13**, 2857–2869.
27 C. W. Rees and T.-Y. Yue, *J. Chem. Soc., Perkin Trans. 1*, 2001, 2538–2542.
28 A. Gieren, V. Lamm, T. Hübner, M. Rabben, R. Neidlein and D. Droste, *Chem. Ber.*, 1984, **117**, 1940–1953.
29 T. Suzuki, Y. Yamashita, T. Fukushima and T. Miyashi, *Mol. Cryst. Liq. Cryst. Sci. Technol., Sect. A*, 1997, **296**, 165–180.
30 N. A. Pushkarevsky, A. V. Lonchakov, N. A. Semenov, E. Lork, L. I. Buravov, L. S. Konstantinova, G. T. Silber, N. Robertson, N. P. Gritsan, O. A. Rakitin, J. D. Woollins, E. B. Yagubskii, J. Beckmann and A. V. Zibarev, *Synth. Met.*, 2012, **162**, 2267–2276.
31 Y. Yamashita, T. Suzuki, G. Saito and T. Mukai, *Chem. Lett.*, 1985, **14**, 1759–1762.
32 M. Tomura and Y. Yamashita, *Molecules*, 2009, **14**, 4266–4274.
33 Y. Misaki, T. Miura, H. Fujiwara, K. Kawakami, T. Yamabe, T. Mori, H. Mori and S. Tanaka, *Synth. Met.*, 1997, **86**, 1821–1822.
34 M. Tomura and Y. Yamashita, *Synth. Met.*, 1997, **86**, 1871–1872.
35 T. Naito, A. Kobayashi, H. Kobayashi and A. E. Underhill, *Chem. Commun.*, 1996, 521–522.
36 A. E. Underhill, I. Hawkins, S. Edge and S. B. Wilkes, *Synth. Met.*, 1993, **56**, 1914–1919.
37 M. Tomura, S. Tanaka and Y. Yamashita, *Heterocycles*, 1993, **35**, 69–72.
38 T. Salzillo, A. Campos and M. Mas-Torrent, *J. Mater. Chem. C*, 2019, **7**, 10257–10263.
39 M. A. Spackman and D. Jayatilaka, *CrystEngComm*, 2009, **11**, 19–32.
40 M. J. Turner, S. Grabowsky, D. Jayatilaka and M. A. Spackman, *J. Phys. Chem. Lett.*, 2014, **5**, 4249–4255.
41 C. F. Mackenzie, P. R. Spackman, D. Jayatilaka and M. A. Spackman, *IUCrJ*, 2017, **4**, 575–587.
42 R. F. W. Bader, *Chem. Rev.*, 1991, **91**, 893–928.
43 E. R. Johnson, S. Keinan, P. Mori-Sánchez, J. Contreras-García, A. J. Cohen and W. Yang, *J. Am. Chem. Soc.*, 2010, **132**, 6498–6506.
44 A. Otero-de-la-Roza, E. R. Johnson and J. Contreras-García, *Phys. Chem. Chem. Phys.*, 2012, **14**, 12165–121721.
45 P. A. Stuzhin, E. M. Bauer and C. Ercolani, *Inorg. Chem.*, 1998, **37**, 1533–1539.
46 E. M. Bauer, C. Ercolani, P. Galli, I. A. Popkova and P. A. Stuzhin, *J. Porphyrins Phthalocyanines*, 1999, **3**, 371–379.
47 A. V. Zibarev and A. O. Miller, *J. Fluorine Chem.*, 1990, **50**, 359–363.
48 A. P. Komin and M. Carmack, *J. Heterocycl. Chem.*, 1976, **13**, 13–22.
49 N. A. Semenov, N. A. Pushkarevsky, J. Beckmann, P. Finke, E. Lork, R. Mews, I. Yu. Bagryanskaya, Yu. V. Gatilov, S. N. Konchenko, V. G. Vasiliev and A. V. Zibarev, *Eur. J. Inorg. Chem.*, 2012, **2012**, 3693–3703.
50 G. M. Sheldrick, *SHELX-97 – Programs for Crystal Structure Analysis (Release 97–2)*, University of Göttingen, Germany, 1997.
51 O. V. Dolomanov, L. J. Bourhis, R. J. Gildea, J. A. K. Howard and H. Puschmann, *J. Appl. Crystallogr.*, 2009, **42**, 339–341.
52 G. M. Sheldrick, *Acta Crystallogr., Sect. C: Struct. Chem.*, 2015, **71**, 3–8.
53 SADABS, *v. 2008-1*, Bruker AXS Inc., Madison, WI, USA, 2008.
54 C. F. Macrae, P. R. Edgington, P. McCabe, E. Pidcock, G. P. Shields, R. Taylor, M. Towler and J. van de Streek, *J. Appl. Crystallogr.*, 2006, **39**, 453–457.
55 S. Grimme, *J. Comput. Chem.*, 2006, **27**, 1787–1799.
56 S. Grimme, J. Antony, S. Ehrlich and H. Krieg, *J. Chem. Phys.*, 2010, **132**, 154104.
57 F. Weigend and R. Ahlrichs, *Phys. Chem. Chem. Phys.*, 2005, **7**, 3297–3305.
58 F. Weigend, *Phys. Chem. Chem. Phys.*, 2006, **8**, 1057–1065.
59 S. Grimme, S. Ehrlich and L. Goerigk, *J. Comput. Chem.*, 2011, **32**, 1456–1465.
60 H. Kruse and S. Grimme, *J. Chem. Phys.*, 2012, **136**, 154101.
61 A. Dreuw and M. Head-Gordon, *Chem. Rev.*, 2005, **105**, 4009–4037.
62 S. Grimme and F. Neese, *J. Chem. Phys.*, 2007, **127**, 154116.
63 S. Sinnecker, A. Rajendran, A. Klamt, M. Diedenhofen and F. Neese, *J. Phys. Chem. A*, 2006, **110**, 2235–2245.
64 A. Klamt and G. Schüürmann, *J. Chem. Soc., Perkin Trans. 2*, 1993, 799–805.
65 S. Kossmann and F. Neese, *J. Chem. Theory Comput.*, 2010, **6**, 2325–2338.
66 F. Neese, F. Wennmohs, A. Hansen and U. Becker, *Chem. Phys.*, 2009, **356**, 98–109.
67 F. Neese, *Wiley Interdiscip. Rev.: Comput. Mol. Sci.*, 2018, **8**, e1327.
68 A. D. Becke, *J. Chem. Phys.*, 1993, **98**, 1372–1377.
69 A. D. Becke, *J. Chem. Phys.*, 1993, **98**, 5648–5652.
70 C. Lee, W. Yang and R. G. Parr, *Phys. Rev. B*, 1988, **37**, 785–789.
71 M. J. Frisch, G. W. Trucks, H. B. Schlegel, G. E. Scuseria, M. A. Robb, J. R. Cheeseman, G. Scalmani, V. Barone, G. A. Petersson, H. Nakatsuji, X. Li, M. Caricato, A. Marenich, J. Bloino, B. G. Janesko, R. Gomperts, B. Mennucci, H. P. Hratchian, J. V. Ortiz, A. F. Izmaylov, J. L. Sonnenberg, D. Williams-Young, F. Ding, F. Lipparini, F. Egidi, J. Goings, B. Peng, A. Petrone, T. Henderson, D. Ranasinghe, V. G. Zakrzewski, J. Gao, N. Rega, G. Zheng, W. Liang, M. Hada, M. Ehara, K. Toyota, R. Fukuda, J. Hasegawa, M. Ishida, T. Nakajima, Y. Honda, O. Kitao, H. Nakai, T. Vreven, K. Throssell, J. A. Montgomery, Jr., J. E. Peralta, F. Ogliaro, M. Bearpark, J. J. Heyd, E. Brothers, K. N. Kudin, V. N. Staroverov, T. Keith, R. Kobayashi, J. Normand, K. Raghavachari, A. Rendell, J. C. Burant, S. S. Iyengar, J. Tomasi, M. Cossi, J. M. Millam, M. Klene, C. Adamo, R. Cammi, J. W. Ochterski, R. L. Martin, K. Morokuma, O. Farkas, J. B. Foresman and D. J. Fox, *Gaussian 09, Revision D.01*, Gaussian Inc., Wallingford CT, 2013.

72 T. Lu and F. Chen, *J. Comput. Chem.*, 2012, **33**, 580–592.

73 W. Humphrey, A. Dalke and K. Schulten, *J. Mol. Graphics*, 1996, **14**, 33–38.

74 P. R. Spackman, M. J. Turner, J. L. McKinnon, S. K. Wolff, D. J. Grimwood, D. Jayatilaka and M. A. Spackman, *J. Appl. Crystallogr.*, 2021, **54**, 1006–1011.

75 J. Tirado-Rives and W. L. Jorgensen, *J. Chem. Theory Comput.*, 2008, **4**, 297–306.

76 N. Godbout, D. R. Salahub, J. Andzelm and E. Wimmer, *Can. J. Chem.*, 1992, **70**, 560–571.

77 C. Sosa, J. Andzelm, B. C. Elkin and E. Wimmer, *J. Phys. Chem.*, 1992, **96**, 6630–6636.

78 S. Alvarez, *Dalton Trans.*, 2013, **42**, 8617–8636.

79 D. D. L. Chung, *J. Mater. Sci.*, 2002, **37**, 1475–1489.

80 E. A. Suturina, N. A. Semenov, A. V. Lonchakov, I. Yu. Bagryanskaya, Yu. V. Gatilov, I. G. Irtegova, N. V. Vasilieva, E. Lork, R. Mews, N. P. Gritsan and A. V. Zibarev, *J. Phys. Chem. A*, 2011, **115**, 4851–4860.

81 L. S. Konstantinova, E. A. Knyazeva, N. V. Obruchnikova, N. V. Vasilieva, I. G. Irtegova, Yu. V. Nelyubina, I. Yu. Bagryanskaya, L. A. Shundrin, Z. Y. Sosnovskaya, A. V. Zibarev and O. A. Rakitin, *Tetrahedron*, 2014, **70**, 5558–5568.

82 A. F. Cozzolino, Q. Yang and I. Vargas-Baca, *Cryst. Growth Des.*, 2010, **10**, 4959–4964.

83 W. F. Cooper, N. C. Kenny, J. W. Edmonds, A. Nagel, F. Wudl and P. Coppens, *J. Chem. Soc. D*, 1971, 889–890.

84 P. Guionneau, D. Chasseau, J. A. K. Howard and P. Day, *Acta Crystallogr., Sect. C: Cryst. Struct. Commun.*, 2000, **56**, 453–454.

85 J. J. McKinnon, M. A. Spackman and A. S. Mitchel, *Acta Crystallogr., Sect. B: Struct. Sci.*, 2004, **60**, 627–668.

86 J. J. McKinnon, A. S. Mitchell and M. A. Spackman, *Chem. – Eur. J.*, 1998, **4**, 2136–2141.

87 M. A. Spackman and P. G. Byrom, *Chem. Phys. Lett.*, 1997, **267**, 215–220.

88 J. J. McKinnon, D. Jayatilaka and M. A. Spackman, *Chem. Commun.*, 2007, 3814–3816.

89 S. J. Grabowski, *Understanding Hydrogen Bonds: Theoretical and Experimental Views*, Royal Society of Chemistry, Cambridge, 2020.

90 S. J. Grabowski, *Phys. Chem. Chem. Phys.*, 2017, **19**, 29742–29759.

91 σ-Holes are regions of low electron density/positive electrostatic potential arising from the anisotropy of the atomic charge distributions and spatially located on the outer-side extensions of the σ-bonds.

92 P. Politzer and J. S. Murray, *Crystals*, 2019, **9**, 165.

93 J. S. Murray, P. Lane, T. Clark, K. E. Riley and P. Politzer, *J. Mol. Model.*, 2012, **18**, 541–548.

94 J. S. Murray, P. Lane, T. Clark and P. Politzer, *J. Mol. Model.*, 2007, **13**, 1033–1038.

95 L. Vogel, P. Wonner and S. M. Huber, *Angew. Chem., Int. Ed.*, 2019, **58**, 1880–1891.

96 D. J. Pascoe, K. B. Ling and S. L. Cockroft, *J. Am. Chem. Soc.*, 2017, **139**, 15160–15167.

97 P. Scilabra, G. Terraneo and G. Resnati, *Acc. Chem. Res.*, 2019, **52**, 1313–1324.

98 N. W. Alcock, *Adv. Inorg. Chem. Radiochem.*, 1972, **15**, 1–58.

99 N. A. Semenov, A. V. Lonchakov, N. A. Pushkarevsky, E. A. Suturina, V. V. Korolev, E. Lork, V. G. Vasiliev, S. N. Konchenko, J. Beckmann, N. P. Gritsan and A. V. Zibarev, *Organometallics*, 2014, **33**, 4302–4314.

100 G. E. Garrett, G. L. Gibson, R. N. Straus, D. S. Seferos and M. S. Taylor, *J. Am. Chem. Soc.*, 2015, **137**, 4126–4133.

101 R. F. W. Bader, *Monatsh. Chem.*, 2005, **136**, 819–854.

102 S. Shahbazian, *Int. J. Quantum Chem.*, 2018, **118**, e25637.

103 S. Shahbazian, *Chem. – Eur. J.*, 2018, **24**, 5401–5405.

104 R. F. W. Bader and H. Essén, *J. Chem. Phys.*, 1984, **80**, 1943–1960.

105 R. G. A. Bone and R. F. W. Bader, *J. Phys. Chem.*, 1996, **100**, 10892–10911.

106 E. Espinosa, I. Alkorta, J. Elguero and E. Molins, *J. Chem. Phys.*, 2002, **117**, 5529–5542.

107 N. A. Pushkarevsky, E. A. Chulanova, L. A. Shundrin, A. I. Smolentsev, G. E. Salnikov, E. A. Pritchina, A. M. Genaev, I. G. Irtegova, I. Yu. Bagryanskaya, S. N. Konchenko, N. P. Gritsan, J. Beckmann and A. V. Zibarev, *Chem. – Eur. J.*, 2019, **25**, 806–816.

108 N. A. Pushkarevsky, P. A. Petrov, D. S. Grigoriev, A. I. Smolentsev, L. M. Lee, F. Kleemiss, G. E. Salnikov, S. N. Konchenko, I. Vargas-Baca, S. Grabowsky, J. Beckmann and A. V. Zibarev, *Chem. – Eur. J.*, 2017, **23**, 10987–10991.

109 N. A. Semenov, D. E. Gorbunov, M. V. Shakhova, G. E. Salnikov, I. Yu. Bagryanskaya, V. V. Korolev, J. Beckmann, N. P. Gritsan and A. V. Zibarev, *Chem. – Eur. J.*, 2018, **24**, 12983–12991.

110 S. Matsuoka, K. Ogawa, R. Ono, K. Nikaido, S. Inoue, T. Higashino, M. Tanaka, J. Tsutsumi, R. Kondo, R. Kumai, S. Tsuzuki, S. Arai and T. Hasegawa, *J. Mater. Chem. C*, 2022, **10**, 16471–16479.

111 R. Pollice and P. Chen, *Angew. Chem., Int. Ed.*, 2019, **58**, 9758–9769.

112 J. P. Wagner and P. R. Schreiner, *Angew. Chem., Int. Ed.*, 2015, **54**, 12274–12296.

113 N. A. Makhaeva, S. A. Amosova and V. A. Potapov, *Molecules*, 2022, **27**, 5613.